Planar Antennas for CubeSat Missions

Tomás S. Almeida, IST, Carlos A. Fernandes, IST, and Jorge R. Costa, ISCTE
Instituto Superior Técnico, Av. Rovisco Pais 1, 1049-001, Lisbon, Portugal
tomas.s.almeida@tecnico.ulisboa.pt

***Abstract*—CubeSats are a type of pico-satellites that have a standardized size of 10 x 10 x 10 cm^3 (1U), or 1U multiples, and weigh less than 1.33 kg per cubic unit. A few challenges arise when designing an antenna to be integrated in the CubeSat's small structure. Miniaturization techniques must be used to shrink antenna size and deployable antennas solutions can be used when bigger antenna apertures are needed e.g., in applications that require a high gain antenna. Also, special challenges arise due to the harsh environment in space. This paper presents two different planar antennas solutions, for CubeSat applications. First, a circularly polarized patch antenna for the ISTsat-1 CubeSat, is developed. Secondly, a reflect array (RA) antenna is developed for a possible ISTsat-2 mission. The antenna for ISTsat-1 operates in the L band, more specifically 1090 MHz, and is for an automatic dependent surveillance - broadcast mission (ADS-B). The second antenna operates in the Ka uplink band of 27 - 31 GHz, and can be used for multiple applications, e.g. fast mobile broadband access. The antenna for ISTsat-1 has 3.1 dB of gain, when integrated onto the CubeSat. Also, it has 16 MHz of bandwidth, centered around 1090 MHz, and an axial ratio of 0.5 MHz with a 4 MHz bandwidth. The RA antenna has 26 dB of gain, at 30 GHz, with a large bandwidth (27.5 - 31 GHz) that covers almost the entire Ka uplink band. The antenna is circularly polarized, with a axial ratio lower than 3 dB throughout the whole band. Both antennas are fabricated in space ready substrates, with good thermal and low outgassing properties.**

***Index Terms*—CubeSat, ISTsat-1, Satellite Antennas, Planar Antennas, Patch Antenna, Reflect Array**

I. Introduction

CubeSats are standardized small satellites, of 10 x 10 x 10 cm^3 (1U), and multiples of this unit. Given their small size and low cost, they are perfect for students or small companies that want to perform space research and testing of ideas that could, in the future, be implemented on larger service providing satellites [1]–[3].

Expected to be launched in 2019, ISTsat-1 is a 1U CubeSat being developed by students of Instituto Superior Técnico (IST). The satellite's main mission is to monitor airplanes using Automatic Dependent Surveillance Broadcast (ADS-B) signals. It is also intended to characterize the Cone of Silence when the aircraft is at the satellite's nadir. Being the cone of silence, the region around the aircraft's zenith where, due to the aircraft antenna's radiation pattern, the coverage is very low, or non existent. To receive the ADS-B signals and guarantee a good communication link, a compact ADS-B antenna, that fits into the small CubeSat structure, had to be developed. The ADS-B antenna presented in this paper is one of the satellite's subsystems developed in-house. The other subsystems include an electric power system, an on-board computer, a communications processor, the ADS-B radio, and the Telemetry, Tracking and Command (TTC) radio and respective Very High Frequency (VHF) and Ultra High Frequency (UHF) antennas, being the TTC antennas, commercial solutions.

This paper also presents a solution for an antenna that works in high frequency (Ka band), capable of being integrated in the CubeSat's structure, designed for High Throughput Satellites (HTS) applications. In inter-satellite communications, antennas with high-gain and high operation frequency are usually required to guarantee high-speed communication links. This is also true for HTS, whose main application is faster mobile broadband access.

There are multiple goals for this work. Regarding ISTsat-1's ADS-B antenna, one goal is to identify the antenna's requirements, by analyzing the mission objectives and limitations. The antenna is designed considering the following mission characteristics, link budget, ADS-B operational frequency and minimum bandwidth, and thermal noise. The antenna also needs to conform with the mission restrictions as, the available volume in the CubeSat, and the operational temperature that the antenna will experience in orbit. Considering the ISTsat-1's mission, its requirements and limitations, the best antenna solution will be identified and fabricated.

For the Ka band antenna, the goal is to develop an antenna solution that is small enough to fit in a 1U CubeSat, has a high gain (>23 dB), and wide bandwidth, ideally to cover the entire Ka uplink band (27 GHz to 31 GHz).

There are many challenges when designing an antenna for CubeSat platforms [4]. One is the limited space available to integrate the antenna and the degradation of performance that comes with it. For some cases, antenna miniaturization techniques [5], [6] are required and for others, deployable antennas [7]–[9] is the only option to fit larger antenna systems into the CubeSat's small structure. For the ISTsat-1 ADS-B antenna there are extra challenges such as, strict bandwidth requirements, resonance frequency variation with temperature, high efficiency requirement, influence of the satellite structure and V/UHF antennas, on the antenna's polarization and radiation pattern. In addition, that it has to be made on a material that can withstand vibrations, that has low outgassing properties, and is temperature stable. For the Ka band antenna, the main challenge is obtaining good antenna performance, in terms of gain, with a compact antenna system that fits into the 1U CubeSat. These stringent requirements make the design of good performing antennas very challenging.

II. Test Methodology

In this work, the measurement and test phase involves some extra steps to ensure good performance of the antennas. The methodology for these specific tests, is explained in this section.

A. Material Permittivity Test

Due to uncertainty on the electrical permittivity value, of the substrate materials used for the planar antennas in this paper, in-house permittivity tests are performed to characterize their complex permittivity. For the ISTsat-1 antenna this is important because small shifts in the substrate's permittivity could translate into critical resonant shifts on the antenna's performance, due to the small bandwidth. This is also important for the Ka band antenna, but these tests will not be used as that antenna has more relaxed requirements in terms of bandwidth.

B. Impedance Test

The antenna's input impedance and correspondent S_{11} values, as a function of frequency, are measured with a Vector Network Analyzer (VNA), in order to evaluate the antenna's resonance within the band of interest. Also, it is important to test the antenna's input impedance under different temperatures, because in the harsh space environment, satellites suffer large temperature variations. Related to the impedance and the substrate losses, the antenna's efficiency is measured using the Wheeler cap method [10].

C. Radiation Pattern Test

The radiation pattern measurement for the ISTsat-1 antenna, is done at IT-IST chamber one, which is an 8.5 m x 4.5 m x 3.6 m anechoic chamber that has a frequency range from 1.8 GHz to 18 GHz. Since the ADS-B band is centered at 1.09 GHz and thus outside of the anechoic chamber's designed frequency band, higher discrepancy between simulations and measurements is expected. For the Ka band antenna, it is used IT-IST's chamber number two, which is an 4 m x 2.5 m x 2.4 m anechoic chamber that has a frequency range from 8 GHz to 110 GHz.

D. Integration with CubeSat Test

The input impedance at room temperature, and radiation pattern measurements are repeated with the CubeSat attached, and afterwards with the VHF and UHF antennas installed to analyze their influence.

E. ADS-B System Test

Specifically for the ISTsat-1 ADS-B antenna, preliminary tests with a commercial ADS-B receiver are performed, to see how the fabricated antenna performs as part of a complete ADS-B system, by analyzing the signals received from passing airplanes.

III. ISTsat-1 Antenna

In this section, the development process of the ISTsat-1 antenna is presented. First, the ISTsat-1 mission and its requirements, regarding the ADS-B antenna is analyzed. Then, the design of the antenna solution, is presented. Finally, the development of one prototype and its simulated and measured results, are also presented.

A. Problem Overview

In the ISTsat-1 ADS-B mission, the satellite receives ADS-B signals from airplanes, calculates multiple statistics from this data, and sends it to ground stations using UHF and VHF bands. The ADS-B antenna system mounted on the airplanes usually consists of two quarter-wave blade antennas, one mounted on top of the fuselage and another on the bottom. These antennas have linear polarization, and their generic radiation pattern is illustrated on figure 1a. When mounted onto the airplane fuselage, the blade antenna's radiation pattern is affected and stops being axial symmetric. This radiation pattern is illustrated in figure 1b. For the top-mounted antenna, its radiation pattern presents a null at the airplane's zenith, causing an area of zero coverage with increasing diameter, at higher altitudes.

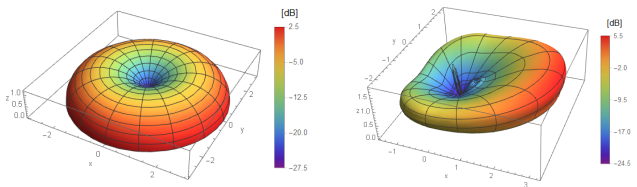

(a) (b)

Fig. 1: Monopole radiation pattern. (a) Ideal, over an infinite ground plane. (b) Mounted on an airplane, adapted from data in [11].

ISTsat-1 will orbit at 400 km of altitude, with the bottom face normal to the Earth's surface, and an expected tumbling rotational speed of 5 degrees/s, in the normal axis. Considering that the UHF and VHF antennas are located in the top of the satellite and the sides covered with solar panels, the only space left to mount the ADS-B antenna for this mission scenario is in the satellite's bottom face. Figure 2 illustrates the ADS-B link scenario, where the satellite's ADS-B antenna is mounted on the bottom face and is communicating with a monopole antenna located on the top of the airplane's fuselage.

The polarization of antennas is an important characteristic, as some polarization configurations can cause higher polarization mismatch, for example with two antennas with orthogonal linear polarizations, where the attenuation due to polarization mismatch is maximum, and thus degrading the communication links. Regarding this mission, circular polarization is found to be the best polarization for the ADS-B antenna. In spite of losing 3 dB in the communication link, due to the mismatch between the linear polarized blade antenna on the airplane and the circular polarized antenna on the ISTsat-1, the circular polarization makes the satellite's ADS-B antenna insensitive

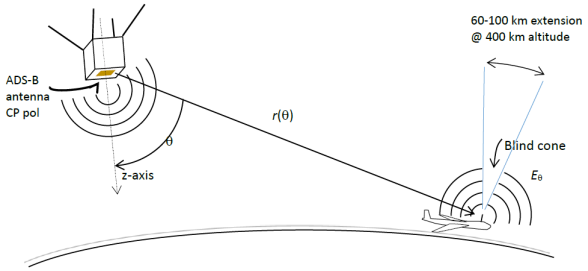

Fig. 2: ADS-B link scenario.

to the position and direction of which the plane is travelling, in regard to polarization.

In this CubeSat mission there are more requirements and challenges that influence the choice of the ADS-B antenna that will be integrated onto ISTsat-1's bottom face. It is important to note that, with all the other subsystems inside the CubeSat, the available space to mount the ADS-B antenna, is only 100 x 100 x 5 mm^3. Even if it is possible to fit a deployable solution in the small volume, this is solution is undesirable for this mission. Deployable solutions would increase the probability of failure and are very challenging to make mechanically robust, which is needed due to the high g-forces and vibrations that the CubeSat will experience upon launch. Additionally, a deployable solution would require extensive reliability tests, which are not compatible with the budget or timeline of this work. There are other issues, like the large temperature variations experienced in space, material outgassing, and the need for more volume inside the CubeSat.

B. Link Budget

The link budget is an important study to be made when working with a wireless communication link. Regarding the ISTsat-1's ADS-B antenna, it is needed to calculate the necessary antenna gain, in order to receive the ADS-B signals. The Friis transmission equation can be used to calculate the power of the signal at the receiving antenna. The power at the receiver is given by,

$$P_r = \frac{P_t G_{sat}(\theta_s, \phi_s) G_{acraft}(\theta_c, \phi_c) \lambda^2}{(4\pi r(\theta_c, \phi_c))^2} c_p c_z L \qquad (1)$$

being P_t the aircraft's transmit power, G_{sat} the satellite's ADS-B antenna gain, G_{acraft} the aircraft's ADS-B antenna gain, λ the ADS-B carrier frequency, $r(\theta_c, \phi_c)$ the line of sight distance between satellite and aircraft, c_p the polarization mismatch loss, c_z the impedance mismatch loss, and L representing the propagation losses.

Equation 1 was rewritten to express G_{sat} in terms of the other variables, in order to calculate the necessary minimal antenna gain for the satellite ADS-B antenna so that the satellite's ADS-B receiver could decode the messages. The considered transmitted power was 500 W, which is the maximum power transmitted by commercial airplanes, and the receiving power was -95 dBm, which is the lowest signal amplitude that the ISTsat-1's ADS-B receiver can receive, also known as sensitivity. Then, for the aircraft's antenna gain, two cases were considered. One, for an ideal monopole and another for the more realistic case, whose radiation patterns are represented on figure 1a and 1b, respectively. The polarization mismatch was chosen as -3 dB to account for the circular/linear polarization mismatch, and the atmospheric losses were not accounted for. Figure 3 illustrates the necessary gain for the ADS-B antenna on an 800 x 800 km^2 area, where each pixel represents the necessary antenna gain for one position of the airplane, for the link budget to be fulfilled.

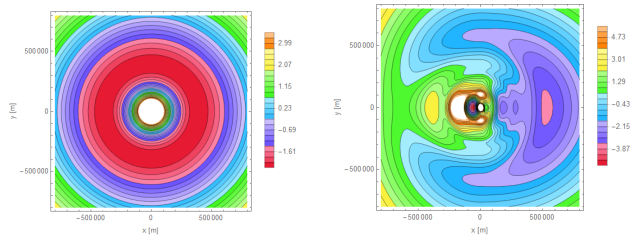

(a) (b)

Fig. 3: Footprint of necessary satellite antenna gain, in dB. (a) Airplane with ideal monopole antenna radiation pattern. (b) Airplane with realistic antenna radiation pattern.

It can be observed, both in figure 3a and 3b, that with an antenna gain of 0 dB, a good coverage of the defined area can be obtained. With this in mind, the proposed antenna solution for the ISTsat-1's ADS-B antenna has to have 0 dB or higher gain. In reality, an antenna gain around 1 - 4 dB would be optimal, to account for possible losses on the communication link.

C. Antenna Design

The circularly polarized patch antenna appears as a good solution, to cope with all the restrictions, presented in the sections above. When designing a circularly polarized patch antenna, many different characteristics must be considered in order to achieve the desired performance. These characteristics include substrate permittivity and height, patch geometry, and feeding technique.

Regarding the substrate electric permittivity, a substrate with a high permittivity ($\epsilon_r > 4$) must be chosen due to the large wavelength at 1090 MHz ($\lambda = 27.5$ cm), comparing with the available space in the 100 x 100 x 5 mm^3 CubeSat bottom face. A substrate with a higher value of permittivity allows for a reduction in the physical size of the antenna, while maintaining its electrical length. This comes at a cost, as higher permittivity substrates usually have higher losses, decreasing the antenna's overall efficiency. Also, the obtained bandwidth is lower compared to lower permittivity substrates, as the fields are more confined in the high permittivity substrate, resulting in poorer radiation by the antenna. For this specific application, a small bandwidth is preferred due to the reduction of temperature noise at the receiver input.

Another antenna parameter that affects the bandwidth is the substrate height, as higher substrates allow for higher bandwidths. The height of the substrate is also related to the antennas efficiency and generally, for electrically small antennas, the efficiency increases with higher substrate heights. However, thicker substrates increase the possibility of exciting surface waves and thus degrading the overall antenna radiation pattern.

There are many techniques and patch geometries to achieve circular polarization. For this antenna it was chosen the square patch with truncated corners, as it is a stable, well known solution, that is well characterized in the literature. The length of the square patch is chosen so that it resonates at the desired frequency, and the truncated corners introduce two degenerate orthogonal modes, ideally 90 degrees out of phase, in order to achieve circular polarization.

Regarding the feeding technique, this antenna needed a low profile, easy to assemble feed, due to the small available space inside the CubeSat. The probe feed presented itself as the best option. Comparing with the microstrip line feed, the probe feed does not need a microstrip line at the patch's surface and also allows to have the connector closer to the center of the patch, away from the ISTsat-1's structural pillars. Another option is the slot feed, but it introduces the added complexity of layer superposition. Due to the antenna height restriction, a low profile connector is used, of the MMCX type.

Lastly, it is important to note that the substrate material used in this application must be space rated and have low outgassing characteristics. The material should also have a low dependency of temperature, regarding its electric and physical properties.

D. Simulations and Measurements

The substrate material chosen for the final prototype is the RT/duroid® 6010, with relative electric permittivity of 10.5. This high permittivity, ceramic-PTFE substrate, has tight ϵ_r and thickness control, low moisture absorption, good thermal mechanical stability, and low outgassing properties, which make it a good choice for space applications. A substrate thickness of 2.5 mm was chosen as the best compromise between high efficiency and low bandwidth. Figure 4 illustrates the designed 3D antenna model and the respective fabricated prototype. The antenna's parameters are specified in table I.

TABLE I: RT6010 patch antenna dimensions in millimeters.

L	L_p	X_{feed}	T_c	C_c	X_S	S_L	S_W
98	41.74	7.3	2.97	8.5	10.1	11.8	1.95

A small slot had to be opened at the edge of the antenna (see figure 4) to allow temporary servicing access to other internal sub-systems after complete system assembling. This is a small slot compared to one wavelength, and therefore the radiation through the slot is minimal and does not affect the subsystems that will be mounted below the antenna. The antenna's reflection coefficient was measured and the results are represented in figure 5.

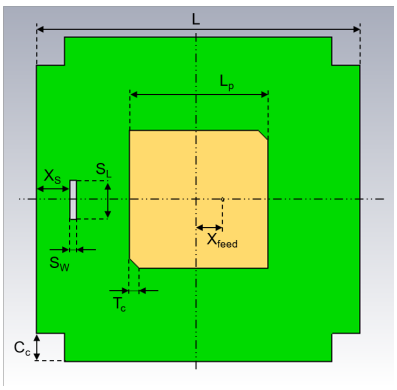

(a)

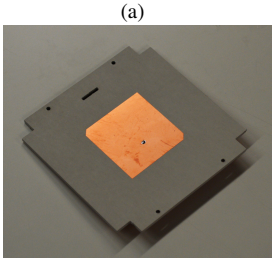

(b)

Fig. 4: Patch antenna with RT6010 substrate. (a) Simulation model. (b) Fabricated prototype.

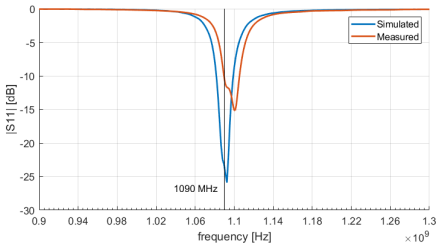

Fig. 5: Comparison between simulated and measured reflection coefficients.

The center resonance frequency of the fabricated prototype is 1095 MHz, which is 5 MHz (0.5% error) up-shifted, comparing with the simulated result. This error is due to the small but present 2.5% uncertainty, on the electric permittivity value. This shift in frequency is not detrimental to the good performance of the antenna. In this case it is actually desirable, as the expected antenna temperature in orbit is well below room temperature, which means that at nominal antenna temperature (0 °C), the resonance frequency will be centered at around 1090 MHz. The obtained bandwidth is 17 MHz and 16 MHz, for the simulated and fabricated antenna, respectively. Figure 6 illustrates the measured and simulated radiation pattern cuts.

There is good agreement between simulated and measured results. The relatively small difference in the cross-polarization component between measurements and simulations is probably due to the limitations of the anechoic chamber. The axial ratio was also measured and is represented in figure 7.

The measured axial ratio is low, being 0.33 dB at 1093 MHz. This is a good result, which means that the antenna has almost pure circular polarization. The axial ratio

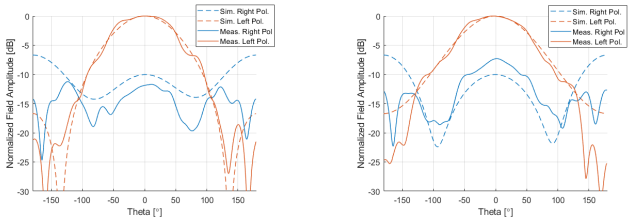

(a) (b)

Fig. 6: Simulated and measured normalized radiation pattern cuts for RT6010 antenna, in free-space. (a) $\phi = 0°$. (b) $\phi = 90°$.

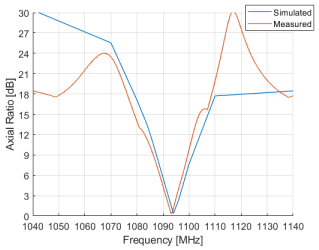

Fig. 7: RT6010 antenna's simulated and measured values of axial ratio, for $\theta = 0°$ and $\phi = 0°$.

bandwidth is approximately 4 MHz, around 1093 MHz.

The efficiency of the antenna was measured and calculated using the Wheeler Cap method [10]. The calculated antenna efficiency at 1090 MHz was approximately 80%. This result is very good, considering the size reduction of the antenna.

The antenna was subjected to temperature cycle tests, to see how the resonance shifted, with the change in temperature. The antenna's reflection coefficient was measured at three different temperatures: cold, room temperature, and hot measurements. Figure 8 illustrates these results.

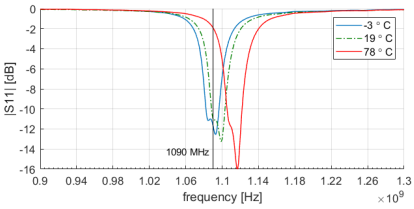

Fig. 8: Variation of the antenna's S11 for three different temperatures.

When the antenna was cooled to -3 °C, its resonance frequency shifted down 6 MHz, and shifted up 18 MHz when it was heated to 78 °C, comparing to the room temperature measurement. This resonance frequency shift, translates into a resonance frequency change per degree of 0.298 MHz/°C. In order to see what was the antenna's operational temperature range in terms of bandwidth, the reflection coefficient curve for 19 °C was extrapolated, using the frequency variation of 0.298 MHz/°C. Figure 9 shows the antenna's reflection coefficient for the minimum and maximum temperatures that result in the ADS-B frequency of 1090 MHz still being within the bandwidth.

The resulting minimum and maximum operational temperatures, so that the ADS-B frequency is inside the antenna's bandwidth, are -25 °C and 25 °C, respectively. This is a wide enough temperature range, that accommodates the expected antenna's temperature in orbit.

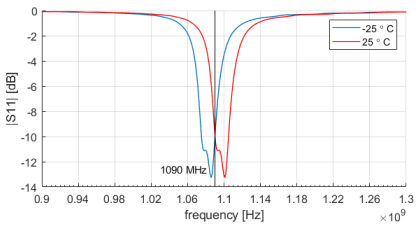

Fig. 9: Antenna's S11 for minimum and maximum operational temperatures.

The antenna was then integrated onto the CubeSat structure, to study its influence. Figure 10 shows a comparison between the radiation pattern of the antenna in free space and the antenna on the CubeSat.

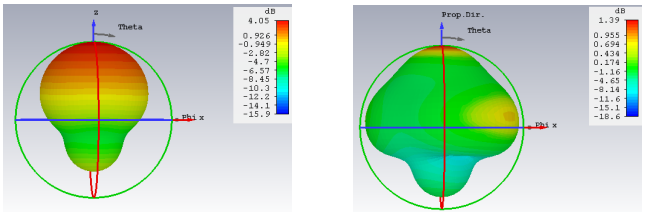

(a) (b)

Fig. 10: RT6010 antenna simulated radiation pattern (gain). (a) Antenna in free space. (b) Antenna with structure.

It can be clearly seen, that there is power that is radiated towards the sides, when the antenna is on the CubeSat. This causes the gain to decrease, which will degrade the communication link. The measured axial ratio is kept low, with a value of 0.22 dB, at 1093 MHz, and a 3 dB bandwidth of 4 MHz.

Upon introducing the VHF and UHF antennas, the ADS-B antenna recovered 1.5 dB of gain, from 1.39 dB to 3.1 dB. The comparison between simulated and measured radiation patterns is illustrated in figure 11.

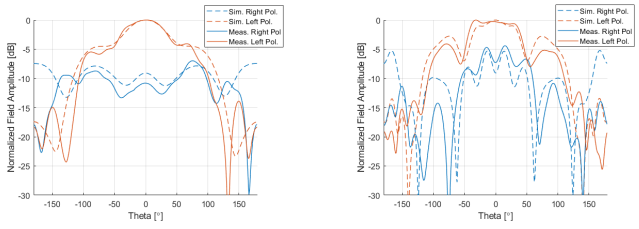

(a) (b)

Fig. 11: Simulated and measured normalized radiation pattern cuts for RT6010 antenna, with the structure and V/UHF antennas. (a) $\phi = 0°$. (b) $\phi = 90°$.

There is a very good agreement between simulation and measurements. With this in mind, the simulated results are validated by the measurements, and the actual antenna gain should be approximately the same as the simulated result.

The axial ratio of the antenna integrated onto the satellite, with the V/UHF antennas, is quite low at 0.5 dB, for 1094 MHz. The 3 dB axial ratio bandwidth is identical to the previous cases, being 4 MHz centered at 1094 MHz. It can be concluded that, the antenna's axial ratio is unaffected, by the inclusion of the CubeSat structure and the V/UHF antennas.

E. Test with ADS-B Receiver

In order to assess the performance of the developed antenna when connected to an ADS-B receiver, the antenna was connected to a commercial ADS-B receiver from uAvionix [12].

Figure 12 illustrates the measurement setup used for the ADS-B receiver test. The antenna is secured on a tripod and connected to the ADS-B receiver, then an USB to serial converter is used to convert the messages to be read out by a computer. The software used to decode the messages is from an open source project called ArduPilot, and the tool used is the mavlogdump, for the mavlink [13].

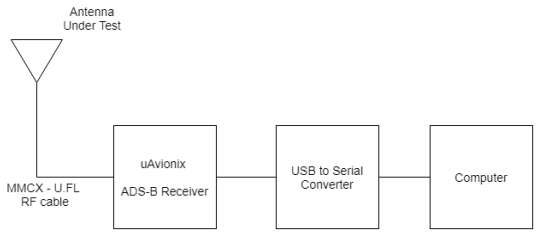

Fig. 12: Diagram of the ADS-B test setup.

The measurements were made from the 12th floor of IST's north tower in Lisbon, in order to favour the line of sight between the airplanes and the antenna. After some preliminary tests it was confirmed that the direction that resulted in best results, meaning more plane signals acquired, was the SW direction. Figure 13 shows the position of the airplanes, retrieved from the ADS-B signals received with the antenna integrated onto the CubeSat structure, with the VHF and UHF antennas.

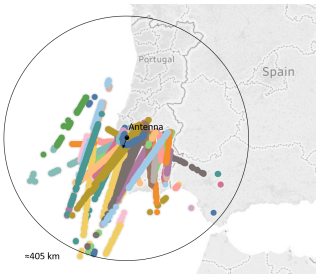

Fig. 13: Airplane signals received with RT6010 antenna on the structure, with VHF and UHF antennas, during 1 hour of measurements.

The approximate range obtained with this setup is around 405 km. The range is limited by the attenuation introduced by the curvature of the Earth, which is noticeable with planes at 10 km of altitude and 400 km of distance. This attenuation will not be present when the satellite will be in orbit. Without this attenuation, it is expected that the range will be closer to the desired 600 km. The message error rate was calculated, where two types of errors were considered. One, where all the messages not containing the airplanes' coordinates was considered an erroneous message. Another, where it was considered an erroneous message when there were no coordinates nor callsign. The message error rate was 18.6% for the first case, and 22.7% for the second.

IV. CubeSat Reflect Array Antenna

A. System Analysis

The objective of the development of this Reflect Array (RA) antenna, was to provide a circularly polarized, high gain antenna solution for the Ka uplink band (27 - 31 GHz), that can be integrated into a 1U CubeSat, for fast mobile broadband access applications. The high gain is needed to compensate for the low power transceivers used for such applications, and also to allow for higher throughput rates. When used for a specific application there should always be a link-budget study, like the one presented in the previous chapter, to understand the necessary antenna gain for a good communication link. The achievable antenna gain is limited by its aperture size and thus there are some challenges when integrating high gain antennas into the small CubeSat structure. With this in mind, a deployable RA antenna that fits into a 1U CubeSat, was developed and fabricated. For this antenna the restriction of not wanting a deployable solution does not apply, as this antenna is not meant to be launched in the immediate future.

The best position to mount a deployable RA antenna on a 1U CubeSat, was found to be the satellite's (nadir) bottom face. This presents itself as the best position due to the side and top faces being usually covered with solar panels. The developed antenna will be integrated on the bottom side of the satellite and will have an aperture area of 10 x 10 cm^2, which corresponds to the bottom face area. The feed antenna for the RA will also be mounted on the bottom face, illuminating the RA aperture. The main idea is that the RA surface can be folded onto the bottom face, over the feed, during stow and launch. When in orbit, the RA surface which is secured by a burn wire and springs at the hinges, will be released and deployed to its operating state. Figure 14 illustrates the general idea for this RA system, integrated on a 1U CubeSat.

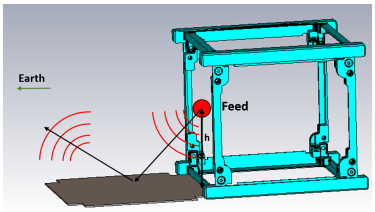

Fig. 14: Reflectarray antenna system in the deployed position, integrated on the bottom face of a 1U CubeSat structure.

The maximum theoretical directivity of an aperture antenna can be defined by

$$D_{max} = \frac{4\pi A_{ap}}{\lambda^2} sin(\alpha), \tag{2}$$

where A_{ap} is the aperture area, λ the wavelength and α the angle of the outgoing wave, radiated by the aperture, with the surface normal. Considering the available space of 10 x 10 cm^2, the wavelength of 1 cm (f = 30 GHz), and an angle of 45° for the output beam, the maximum theoretical directivity is 29.5 dB. The output angle was chosen as 45°, because it is halfway between the normal and tangential directions, while still pointing at the Earth, for an orbit of 400 km of altitude. Considering a -3dB beamwidth of 8° and -10 dB beamwidth of 14°, the approximated ground coverage diameter would be 56 km and 200 km, respectively, for an orbit of 400 km of altitude.

B. Phase Distribution

In order to achieve beam collimation, the RA must introduce the necessary phase shift. This phase shift cannot be implemented in a continuous manner throughout the surface, as the use of unit cells imply a spacial discretization of the phase. Smaller unit cells will allow for a better discretization. Usually, as a rule of thumb, the size of the unit cells should be smaller than one wavelength. Figure 15 illustrates a generic RA system, with a feed and an arbitrary number of cells.

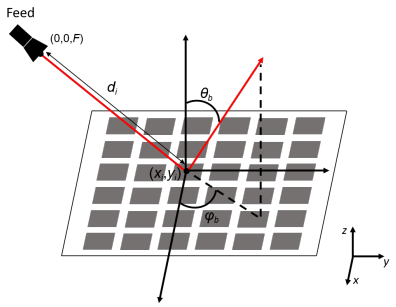

Fig. 15: Reflect array antenna diagram, with offset feed.

In order to obtain a beam with a certain tilt angle of (θ_i, ϕ_i), the phase distribution must be

$$\Phi(x_i, y_i) = -k_0[sin(\theta_b)cos(\phi_b)x_i - sin(\theta_b)sin(\phi_b)y_i], \quad (3)$$

where k_0 is the free space wavenumber, and (x_i, y_i) a point in the aperture surface. In the case of the RA, the unit cells must introduce a phase shift that accounts for the different path lengths between the feed and each cell. The phase at the RA surface, after reflection of the beam, can be defined by

$$\Phi(x_i, y_i) = -k_0 d_i + \Phi_{uc}(x_i, y_i), \quad (4)$$

where d_i is the distance between the feed phase center and each unit cell, and $\Phi_{uc}(x_i, y_i)$ the phase shift introduced by each unit cell. After equating equation 4 to 3 and choosing ϕ_i = 0°, for this specific RA antenna system, the needed phase shift that each cell must induce is defined by

$$\Phi_{uc}(x_i, y_i) = k_0 d_i - k_0 x_i sin(\theta_b). \quad (5)$$

It was chosen a feed height of h = 50 mm, positioned at the border of the RA, with an input and output beam angle of 45°. The necessary phase distribution can be calculated with equation 5, and is represented in figure 16.

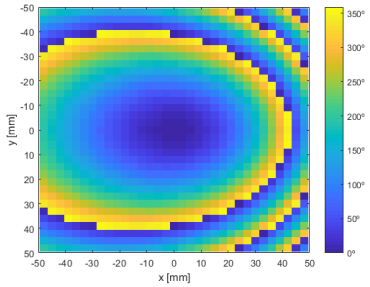

Fig. 16: Necessary phase shift to achieve beam collimation. Each pixel represents one 3 x 3 mm^2 unit cell.

In the next section, the unit cell design to achieve the necessary phase shift, is presented.

C. Reflect Array Preliminary Simulations

A first approximation of the antenna's directivity and radiation pattern was obtained using a hybrid geometrical optics/physical optics tool, called KH3D [14]. This tool calculates the radiation pattern of an arbitrary aperture, by considering the amplitude and phase of the tangential field component at the aperture surface, originated from the feed. The use of this tool allows easy optimization of the RA system, in terms of feed position and gain, as this method is quite light regarding computational power, compared to the full-wave simulations that are required in a later development phase. Good results were obtained when h = 50 mm, with the feed in the middle point of the CubeSat face, pointing towards the centre of the RA surface, with gain of 11 dB and a -3 dB beamwidth of 33°. The feed gain of 11 dB was chosen as a compromise between energy spillover and uniform illumination. The calculated radiation pattern, using the physical optics tool, is illustrated in figure 17.

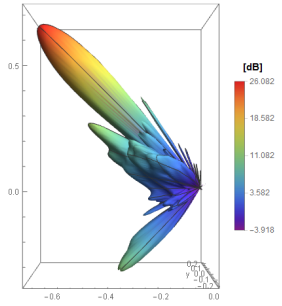

Fig. 17: Calculated radiation pattern of 10 x 10 cm^2 reflectarray.

There is a well defined beam with 45° of tilt and approximately 26.1 dB of directivity. Considering the maximum theoretical directivity of 29.5 dB, the resulting theoretical aperture efficiency is approximately 45.7%.

D. Unit Cell Design

The unit cells designed for this RA antenna consist of two concentric square ring resonators. This unit cell design proved to be a good option for this application, as the obtained phase shift at 30 GHz covered the whole 0° to 360° range. The unit cell is 3 x 3 mm^2 and the phase shift is obtained by varying the outer ring resonator's side length, and consequently the inner ring side length as well. Figure 18 illustrates one unit cell with a specific outer ring side length, and its parameters are specified in table II.

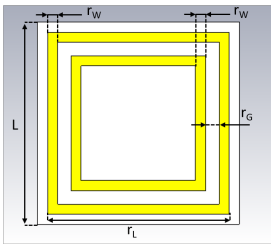

Fig. 18: Unit cell geometry.

TABLE II: Unit cell dimension parameters in millimeters.

L	r_W	r_G
3	0.15	0.2

The substrate used for these unit cells was RT/duroid® 5880, with a thickness of 0.787 mm, ϵ_r = 2.2 and tan δ = 0.0009. This is a space rated substrate with low outgassing properties, low thermal coefficients and quite low losses.

The unit cells were simulated and optimized by full-wave analysis using CST-MWS [15], with the frequency domain solver. In order to reduce the simulation and optimization time, the scattering matrix was obtained for an infinite periodic structure of the same unit cell. This stands as a good approximation when designing unit cells, to obtain the introduced phase shift with the change of a design parameter. Figure 19 shows the reflection coefficient for these unit cells for different values of r_L, between 1.1 and 2.7 mm.

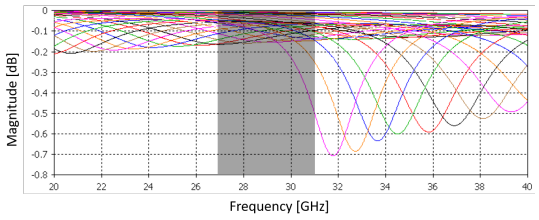

Fig. 19: S11 magnitude of the designed unit cell. Each color represents a different outer ring length.

The resulting reflection coefficient is quite high, (-0.5 to -0.16 dB) within the band of interest. This is good, as a high reflection coefficient means that almost all power that is incident on the RA surface, is reflected back. In terms of the phase response, the phase shift introduced by the cell was analyzed for an outer ring lengths from 1.1 to 2.7 mm, with steps of 0.1 mm. The phase shift was also analyzed for different incidence angles, ranging from 0° to 60°. Figure 20 illustrates the S-shaped curve of the introduced phase shift in terms of the outer ring length, for different incident angles.

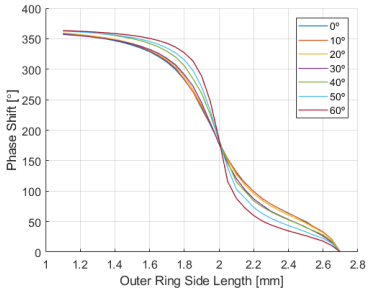

Fig. 20: Unit cell's reflection coefficient phase for different outer ring side lengths, and different incidence angles.

The obtained phase shift covers the whole 360° range (-250° to 100°). There is a noticeable difference on the S-curves when the incidence angle is higher than 40°. Because of this, the incidence angle will be taken into account when matching a certain outer ring length to a necessary phase shift. This decision of including the incidence angle will not improve the RA antenna's gain, but it will lower the side lobe levels.

E. Reflect Array Simulations

The next step, after designing the unit cells, consists in designing the whole RA surface. The results in figure 20, for each incidence angle, consist of discrete values with a step size of 0.1 mm. In order to obtain a continuous function with the phase shift depending on the outer ring length, a polynomial fit of 10th order was used, for each S-curve. It was then possible to assign a specific outer ring length to a necessary phase shift, represented in figure 16.

The RA surface consists of 1089 cells like the one in figure 18, with changing outer ring lengths. The corners of the 10 x 10 cm^2 RA surface where cut in order to fit into the small 1U CubeSat bottom face, between the structural pillars. In this work, a horn antenna was used instead of a planar feed solution. The horn antenna feed has 10.8 dB of gain at 30 GHz. Two simulations were performed with the horn antenna in two orthogonal positions, in order to emulate a circularly polarized feed by post-processing. The horn antenna is not intended to be the feed for this RA system as it is relatively large at these frequencies, which means that it will protrude the 1U CubeSat's bottom face. Despite this, the horn antenna serves perfectly to test the developed RA surface, as it does not change the fundamental concept, nor the validity of the demonstration. Also, the design and fabrication of a planar, circularly polarized, tilted beam feed array, is outside of the scope of this work.

The RA antenna was simulated using the time domain solver of CST-MWS. Figure 21 shows the simulated farfield results for both rotations of the feed.

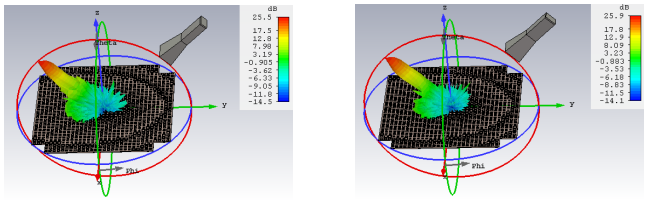

(a) (b)

Fig. 21: Simulated radiation pattern results. (a) Feed in horizontal position. (b) Feed in vertical position.

The gain obtained, using full-wave simulations, matches perfectly with the predicted results using the physical optics tool. In order to represent the radiation pattern in the two orthogonal circular polarized field components, it must be converted from the linear polarized representation. The left circularly polarized component can be defined by

$$L = \frac{E^{\theta\theta} + jE^{\phi\theta} + E^{\phi\phi} - jE^{\theta\phi}}{2}, \tag{6}$$

where $E^{\theta\theta}$ and $E^{\phi\theta}$ are the E^{θ} and E^{ϕ} field components with the feed in the position of figure 21a, respectively. $E^{\theta\phi}$ and $E^{\phi\phi}$ are the E^{θ} and E^{ϕ} field components with the feed in the position of figure 21b. Similarly, the right circularly polarized component can be defined by

$$R = \frac{E^{\theta\theta} + jE^{\phi\theta} - E^{\phi\phi} + jE^{\theta\phi}}{2}, \tag{7}$$

with all the variables defined above. Figure 22 shows a cut for Phi = 90°, of the simulated radiation pattern, represented with circularly polarized components.

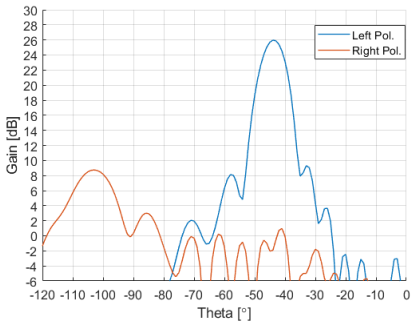

Fig. 22: Radiation pattern cut for Phi = 90°. The angle Theta = -90° corresponds to normal incidence on the Earth's surface.

The obtained realized gain is 26 dB, at Theta = -44°. The cross-polarization is low at -28 dB, and the side lobe level is -16.7 dB.

F. Fabricated Prototype and Measurements

The designed RA antenna was fabricated, and special supports were 3D printed, in order to mount the RA surface and feed to the already built CubeSat structure, the same used in the previous chapter. Figure 23 illustrates the fabricated prototype, integrated into the 1U CubeSat structure.

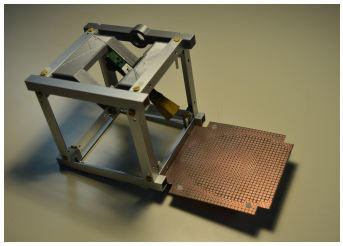

Fig. 23: Fabricated reflect array antenna, integrated into a CubeSat structure.

For the purpose of this paper, a fixed mount for the RA array antenna was built, as the development of a deployable mechanism was outside of the scope of this paper. Despite this, the RA surface was developed with a specific size and geometry so it can, in the future, be integrated into such system.

The fabricated RA antenna's radiation pattern was measured in IT-IST's anechoic chamber number two, and the results are represented in figure 24.

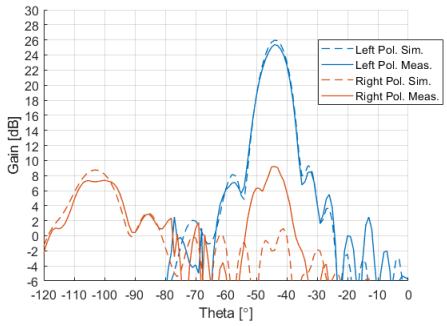

Fig. 24: Measured and simulated radiation pattern cuts for Phi = 90°.

There is a good agreement between measured and simulated results. The measured gain is 25.4 dB, at Theta = -44°. The measured value is 0.6 dB lower than the simulated one. This is though, a very small difference and can be due to small errors on the anechoic chamber measurement or in the numerical methods. The side lobe level is -16.9 dB and the cross-polarization level is -16.2 dB. The measured cross-polarization level at Theta = -44°, is 11.1 dB higher than the simulated value. This is probably caused by the presence of the CubeSat structure in the measurements. The simulations did not include the structure because this is a very demanding simulation and there was not enough computer power to perform them. From the cross-polarization level, the axial ratio was calculated for different frequencies within the Ka uplink band, and it is represented in figure 25.

Both in the simulated and measured results, the axial ratio is below 3 dB, for the band of interest. This confirms that the developed RA antenna is indeed circularly polarized. The antenna gain in the frequency band of interest was also measured, and is illustrated in figure 26.

The -3 dB bandwidth does not cover the whole band, and is from approximately 27.5 GHz to 31 GHz, within the band of interest. However, the fabricated antenna's gain is quite high,

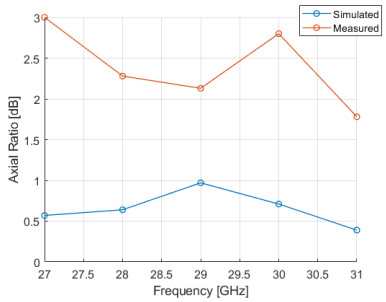

Fig. 25: Measured and simulated axial ratio for Theta = -45°.

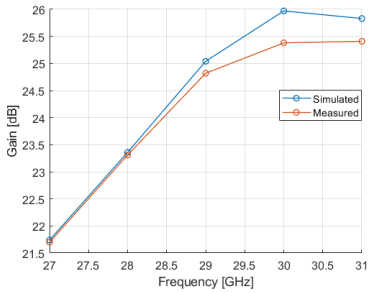

Fig. 26: Measured and simulated gain for Theta = -45°, in the Ka uplink band.

and it decays slowly close to the resonance frequency of the unit cells (30 GHz). In order to get a better distribution of antenna gain through the whole Ka uplink band, the cells should have been designed to the center band frequency (29 GHz).

V. Conclusions

In this work, two different antennas for two different CubeSat missions were developed. One for an ADS-B mission for ISTsat-1 and another for fast mobile broadband access applications, in the Ka band. The ADS-B antenna, developed for ISTsat-1, consisted in a circular polarized patch antenna. The antenna was developed following the strict requirements, of limited space, small bandwidth, high enough gain, thermal and mechanically robustness, and designed to work when integrated into the CubeSat. The resulting antenna proved to be a very good solution for this mission, being fabricated in a space rated material, with low outgassing properties. It has a resonance center frequency of 1090 MHz, at 0 °C, and a small bandwidth of 16 MHz. It can operate within its bandwidth, between -25 °C and 25 °C. It is circular polarized, with a low axial ratio of 0.5 dB, at the resonance frequency. Finally, when mounted onto the CubeSat, it maintains a good gain of 3.1 dB, more than enough to receive the airplanes' signals, at 400 km of distance. In the development of this antenna, new tests were performed, such as the antenna performance study under large temperature changes. Also, an extensive study of how an 1U CubeSat structure affects the antenna performance, of a planar antenna mounted on one face, is also presented. Finally, it is presented a novel deployable wire solution that improves the planar antenna's gain.

The developed RA antenna for the Ka band was a novel solution, for this size of CubeSat, and consisted of a circularly polarized solution with high gain, made to be integrated into the small 1U CubeSat structure. The resulting performance of this antenna was very good, considering the small space available. The developed RA antenna is of the deployable type, and it achieved 26 dB of gain, at the resonance frequency of 30 GHz, with a large 3 dB gain bandwidth that covers almost the whole Ka uplink band. These are good results, as it allows for the antenna to be used in HTS, with multiple applications, for the Ka uplink band.

VI. Acknowledgements

The authors would like to thank Mr. Carlos Brito and Mr. Farinha for the fabrication of prototypes, and António Almeida for the design and fabrication of the supports and prototypes, and measurements.

References

[1] W. Blackwell, G. Allen, C. Galbraith, T. Hancock, R. Leslie, I. Osaretin, L. Retherford, M. Scarito, C. Semisch, M. Shields, M. Silver, D. Toher, K. Wight, D. Miller, K. Cahoy, and N. Erickson, "Nanosatellites for earth environmental monitoring: The micromas project," in *2012 12th Specialist Meeting on Microwave Radiometry and Remote Sensing of the Environment (MicroRad)*, March 2012, pp. 1–4.

[2] M. W. Smith, S. Seager, C. M. Pong, J. S. Villaseñor, G. R. Ricker, D. W. Miller, M. E. Knapp, G. T. Farmer, and R. Jensen-Clem, "Exoplanetsat: detecting transiting exoplanets using a low-cost cubesat platform," in *SPIE Astronomical Telescopes + Instrumentation*. International Society for Optics and Photonics, 2010, pp. 773 127–773 127.

[3] A. Marinan, A. Nicholas, and K. Cahoy, "Ad hoc cubesat constellations: Secondary launch coverage and distribution," in *2013 IEEE Aerospace Conference*, March 2013, pp. 1–15.

[4] S. Gao, K. Clark, M. Unwin, J. Zackrisson, W. A. Shiroma, J. M. Akagi, K. Maynard, P. Garner, L. Boccia, G. Amendola, G. Massa, C. Underwood, M. Brenchley, M. Pointer, and M. N. Sweeting, "Antennas for modern small satellites," *IEEE Antennas and Propagation Magazine*, vol. 51, no. 4, pp. 40–56, Aug 2009.

[5] C. G. Kakoyiannis and P. Constantinou, "A compact microstrip antenna with tapered peripheral slits for cubesat rf payloads at 436mhz: Miniaturization techniques, design and numerical results," in *2008 IEEE International Workshop on Satellite and Space Communications*, Oct 2008, pp. 255–259.

[6] H. Iwasaki, "A circularly polarized small-size microstrip antenna with a cross slot," *IEEE Transactions on Antennas and Propagation*, vol. 44, no. 10, pp. 1399–1401, Oct 1996.

[7] J. Costantine, Y. Tawk, C. G. Christodoulou, J. Banik, and S. Lane, "Cubesat deployable antenna using bistable composite tape-springs," *IEEE Antennas and Wireless Propagation Letters*, vol. 11, pp. 285–288, 2012.

[8] D. Ochoa, K. Hummer, and M. Ciffone, "Deployable helical antenna for nano-satellites," in *Proceedings of the 28th Annual AIAA/USU Conference on Small Satellites*, August 2014, pp. 1–7.

[9] L. Alminde, K. Kaas, M. Bisgaard, J. Christiansen, and D. Gerhardt, "Gomx-1 flight experience and air traffic monitoring results," *Small Satellite Conference*, 2014.

[10] H. A. Wheeler, "The radiansphere around a small antenna," *Proceedings of the IRE*, vol. 47, no. 8, pp. 1325–1331, Aug 1959.

[11] R. Van Der Pryt and R. Vincent, "A simulation of the reception of automatic dependent surveillance-broadcast signals in low earth orbit," *International Journal of Navigation and Observation*, vol. 2015, 2015.

[12] uavionix website. [Online]. Available: https://uavionix.com/products/pingrx/

[13] Mavlink source code. [Online]. Available: https://github.com/ArduPilot/mavlink

[14] C. A. Fernandes, "Kh3d_near. Users manual, Version 0.2g," *Instituto de Telecomunicaes - IST*, Feb 2018.

[15] CST - Computer Simulation Technology. [Online]. Available: www.cst.com